
Probabilistic predictions with Fourier neural operators

Anonymous Author(s)

Affiliation

Address

email

Abstract

1 Neural networks have been successfully applied in modeling partial differential
2 equations, especially in dynamical systems. Commonly used models, such as
3 neural operators, are performing well at deterministic prediction tasks, but lack a
4 quantification of the uncertainty inherent in many complex systems, for example
5 weather forecasting. In this paper, we explore a new approach that combines Fourier
6 neural operators with generative modeling based on strictly proper scoring rules
7 in order to create well-calibrated probabilistic predictions of dynamical systems.
8 We demonstrate improved predictive uncertainty for our approach, especially in
9 settings with very high inherent uncertainty.

10 1 Introduction

11 Many complex phenomena in the sciences are described via time-dependent partial differential
12 equations (PDEs), making their study a crucial research topic. Recent developments in machine
13 learning led to an effective class of neural networks for solving PDEs, called neural operators
14 [Kovachki et al., 2023]. In dynamical systems, these models aim to learn the operator that maps
15 an initial system state to the corresponding solution across time and have been applied to problems
16 such as weather forecasting [Pathak et al., 2022] or fluid dynamics [Renn et al., 2023]. However,
17 neural operators are usually studied in the context of deterministic predictions, not accounting for the
18 inherent uncertainty in complex and chaotic dynamical systems. Several methods have been proposed
19 to enhance neural network architectures to quantify uncertainty. While some approaches focus
20 on perturbing initial conditions [Pathak et al., 2022], many approaches are applied to the network
21 post-hoc. These include statistical post-processing [Bülte et al., 2024] or Bayesian methods [Gal
22 and Ghahramani, 2016]. For neural operators, which learn an output in function space, uncertainty
23 quantification can be more complex. Gal and Ghahramani [2016] propose to generate samples from a
24 posterior predictive distribution by utilizing dropout in the model inference phase. Weber et al.
25 [2024] and Magnani et al. [2024] use a Laplace approximation for the Fourier neural operator, which
26 utilizes a linearized neural network to generate a tractable posterior distribution in function space.

27 In the context of spatial predictions, especially weather forecasting, methods based on the notion
28 of proper scoring rules are commonly applied and have shown to work very well in combination
29 with neural networks [Pacchiardi et al., 2024, Chen et al., 2024]. However, this has not yet been
30 transferred to the setting of operator learning, which requires additional analysis of the corresponding
31 scoring rules in infinite dimensional spaces. In this paper, we utilize proper scoring rules in separable
32 Hilbert spaces in order to train a neural operator to estimate a predictive distribution over functions.
33 We theoretically prove that this is well-motivated by showing that the energy score is strictly proper in
34 infinite dimensional spaces. Our primary aim is to demonstrate the advantages of the approach in pre-
35 dicting dynamical systems. Our approach, which we refer to as probabilistic Fourier neural operator
36 (PFNO), leads to better-calibrated predictive distributions and adequate uncertainty representations
37 even for long dynamical trajectories.

38 **2 Neural operators**

39 The aim of operator learning is to utilize a neural network to learn a mapping between two function
 40 spaces from a finite collection of input-output pairs. Consider an operator $\mathcal{G} : \mathcal{A} \rightarrow \mathcal{U}$, acting on two
 41 separable Banach spaces of functions. A neural operator is a map $\mathcal{G}_\theta : \mathcal{A} \rightarrow \mathcal{U}$, that is parametrized
 42 by finitely many weights $\theta \in \mathbb{R}^p$ and trained on observational data $\{(a_n, u_n)\}_{n=1}^N$, which aims to
 43 approximate the operator \mathcal{G} . Here, a_n is usually an initial system state and u_n is the solution state
 44 of the PDE after some time T . The most commonly used architecture is the Fourier neural operator
 45 (FNO) [Li et al., 2021], which acts on an input function a by specifying several layers of integral
 46 kernels that are parametrized in Fourier space. By utilizing the convolution theorem, one so-called
 47 Fourier block is given as

$$G_i v_i(x) = \sigma(\mathcal{F}^{-1}(R_i \cdot \mathcal{F}(v_i)))(x) + W_i v_i(x), \quad (1)$$

48 where \mathcal{F} and \mathcal{F}^{-1} are the Fourier transform and its inverse. Here, the matrix-valued functions R_i
 49 are directly parametrized in the Fourier domain as neural network weights. The whole network is
 50 specified as a combination of several Fourier blocks with some additional lifting and projection
 51 functions.

52 **3 Probabilistic predictions using neural operators**

53 The method we propose is based on generating a predictive distribution via a sample-based empirical
 54 distribution. We denote the initial condition and the solution of the PDE as a and u , respectively, the
 55 spatio-temporal domain as \mathcal{D} and the empirical predictive distribution, for a fixed initial condition
 56 a , as $\hat{P}_\theta^M = \{\hat{u}^m\}_{m=1}^M$ with samples \hat{u}^m for $m = 1, \dots, M$. For this analysis, we restrict ourselves
 57 to data from separable Hilbert spaces, which includes most solution spaces of PDEs, such as the
 58 Sobolev space $H^k, k \in \mathbb{N}$.

59 **Scoring rule minimization** A scoring rule S is a function that assigns a real-valued score to the
 60 fit between a probability distribution and a corresponding observation [Gneiting and Raftery, 2007].
 61 Define the so-called *expected score* as $S(Q, P) := \mathbb{E}_{X \sim P}[S(Q, X)]$. The scoring rule is called
 62 *proper* with respect to a class of probability measures \mathcal{P} if $S(P, P) \leq S(Q, P), \forall P, Q \in \mathcal{P}$ and it is
 63 called *strictly proper* if equality implies $P = Q$. In other words, a scoring rule is strictly proper if the
 64 true distribution of the observation uniquely minimizes the expected score. More details on proper
 65 scoring rules can be found in Appendix A. Here, we focus mainly on the well-known *energy score*
 66 [Gneiting and Raftery, 2007], which is defined as

$$\text{ES}(P, x) := \mathbb{E}_P[\|X - x\|_{\mathcal{H}}] - \frac{1}{2} \mathbb{E}_P[\|X - X'\|_{\mathcal{H}}], \quad (2)$$

67 where $X, X' \stackrel{\text{i.i.d.}}{\sim} P, x \in \mathcal{H}$ and \mathcal{H} is a separable Hilbert space. Pacchiardi et al. [2024] show how
 68 generative neural networks can be trained via scoring rule minimization in the finite-dimensional
 69 setting. Consider data observation pairs of the form $(a_i, u_i)_{i=1}^n$, where $a_i \sim P_{\mathcal{A}}$ and $u_i \sim P_{\mathcal{U}}$ follow
 70 some distributions over a separable Hilbert space and let $P_\theta(\cdot | a)$ denote an approximate posterior
 71 generated by the network. In the conditional data setting, we assume that $u_i \sim P^*(\cdot | a_i)$. For a
 72 (strictly) proper scoring rule, the minimization objective is given as

$$\operatorname{argmin}_{\theta} \mathbb{E}_{a \sim P_{\mathcal{A}}} \mathbb{E}_{u \sim P^*(\cdot | a)} S(P_\theta(\cdot | a), u)$$

73 and leads to $P_\theta(\cdot | a) = P^*(\cdot | a)$ almost everywhere. In the finite data setting, this objective is
 74 approximated with a Monte Carlo estimator. While closed-form expressions of S are not always
 75 available, the energy score has a representation that admits an unbiased estimator, which requires
 76 the output from our neural network to consist of multiple samples of the predictive distribution, e.g.
 77 $(\hat{u}^m)_{m=1}^M \sim P_\theta(\cdot | a)$. In our case, the minimization objective for the neural network with the energy
 78 score then becomes

$$\operatorname{argmin}_{\theta} \frac{1}{n} \sum_{i=1}^n \left(\frac{1}{M} \sum_{m=1}^M \|\hat{u}_i^m - u_i\|_{\mathcal{H}} - \frac{1}{2M(M-1)} \sum_{\substack{m, h=1 \\ m \neq h}}^M \|\hat{u}_i^m - \hat{u}_i^h\|_{\mathcal{H}} \right). \quad (3)$$

79 In this paper, we extend this approach to the infinite-dimensional setting of neural operators. This
80 is mathematically motivated, as we prove in Appendix A that the energy score is strictly proper
81 in separable Hilbert spaces, which allows network training via scoring rule minimization. As the
82 base architecture we utilize FNOs, and refer to our approach as probabilistic Fourier neural operator
83 (PFNO). In order to create an empirical distribution as the network output, we focus on utilizing
84 stochastic forward passes via dropout [Gal and Ghahramani, 2016]. To further account for the
85 structure of the FNO, we apply additional dropout over the parameters in Fourier space, which then
86 acts globally on the network prediction. The PFNO has the advantage that it is easy to implement
87 in an existing architecture and creates a nonparametric predictive distribution, allowing for more
88 flexibility. We compare the PFNO against the MCDropout and Laplace approximation as baselines.

89 **Baselines:** Gal and Ghahramani [2016] show that a neural network with dropout before each layer
90 is mathematically equivalent to a variational approximation of a Gaussian process. This leads to
91 a simple and efficient way of creating a predictive distribution, referred to as MCDropout. In our
92 setting, the predictive distribution is given as

$$\hat{P}_\theta^M = \{\mathcal{G}_\theta^*(a, \omega_m)\}_{m=1}^M, \quad (4)$$

93 where ω_m is the random dropout variable and \mathcal{G}_θ^* denotes a neural operator trained.

94 Weber et al. [2024] propose to utilize the Laplace approximation (LA) for FNOs, which is based
95 on building a second-order approximation of the weights around the maximum a posteriori (MAP)
96 estimate. By assuming a Gaussian weight prior, the weight-space uncertainty of the LA is given by

$$p(\theta, \mathcal{C}) \approx \mathcal{N}(\theta; \theta_{\text{MAP}}, \Sigma), \quad \Sigma := -(\nabla_\theta^2 \mathcal{L}(\mathcal{C}; \theta)|_{\theta_{\text{MAP}}})^{-1}, \quad (5)$$

97 where $\mathcal{C} = \{(a_n, u_n)\}_{n=1}^N$. The corresponding predictive distribution in function space is an
98 analytically available Gaussian and is used to generate M predictive samples. In contrast to the
99 PFNO, both methods quantify uncertainty for an already trained neural operator.

100 4 Experimental results

101 We analyze our methods on two highly uncertain dynamical systems. First, the Kuramoto-Sivashinsky
102 (KS) equation, which is a one-dimensional chaotic fourth-order parabolic PDE, described by

$$\partial_t u(x, t) + u \partial_x u(x, t) + \partial_x^2 u(x, t) + \partial_x^4 u(x, t) = 0, \quad u(x, 0) = u_0(x). \quad (6)$$

103 We generate 10,000 samples (10% for validation/evaluation) over the domain $\mathcal{D} = [0, 100] \times [0, 300]$.
104 In addition, we evaluate the models on a 2-meter surface temperature prediction task, where we
105 utilize the ERA5 dataset, provided via the WeatherBench benchmark [Rasp et al., 2024] with a spatial
106 resolution of 0.25° across Europe and a time resolution of $6h$. We use data from 2011-2022 with the
107 last two years as validation and test data respectively. For the KS data the model takes and predicts
108 20 timesteps, for the ERA5 it takes and predicts 10 timesteps (60 hours). For evaluation, we consider
109 the following metrics:

$$\text{RMSE}(\hat{P}_\theta^M, u) = \|\bar{u}_M - u\|_{L^2}, \quad (7)$$

$$\text{ES}(\hat{P}_\theta^M, u) = \frac{1}{M} \sum_{m=1}^M \|\hat{u}^m - u\|_{L^2} - \frac{1}{2M(M-1)} \sum_{m \neq h}^M \|\hat{u}^m - \hat{u}^h\|_{L^2}, \quad (8)$$

$$\mathcal{C}_\alpha(\hat{P}_\theta^M, u) = \int_{\mathcal{D}} \mathbb{1} \left\{ u(x, t) \in [\hat{q}_\theta^{\alpha/2}(x, t), \hat{q}_\theta^{1-\alpha/2}(x, t)] \right\} dx dt, \quad (9)$$

Table 1: Evaluation metrics on the Kuramoto-Sivashinsky equation and the 2-meter surface temperature. The best model is highlighted in bold.

		Validation data			Test data		
		RMSE	ES	$\mathcal{C}_{0.05}$	RMSE	ES	$\mathcal{C}_{0.05}$
KS	PFNO	0.8674	0.6108	0.8781	0.8677	0.6110	0.8774
	MCDropout	0.8446	0.7298	0.3595	0.8457	0.7310	0.3580
	Laplace	0.8352	0.8247	0.0197	0.8359	0.8250	0.0207
T2M	PFNO	0.1677	0.1182	0.9427	0.3291	0.2427	0.7865
	MCDropout	0.1834	0.1427	0.6325	0.3035	0.2535	0.4284
	Laplace	0.1910	0.1421	0.3231	0.3145	0.2491	0.2387

110 where \bar{u}_M denotes the mean prediction, and \hat{q}_θ^α denotes the empirical α quantile of the predictive
 111 distribution. All metrics are then averaged over the validation or test dataset. The RMSE evaluates
 112 the match between the mean of the predictive distribution and the observation, while the energy
 113 score evaluates the match for the predictive distribution as a whole. The coverage \mathcal{C}_α is calculated
 114 pointwise and describes, whether the predictive $1 - \alpha$ interval entails the true value. It should be
 115 close to $1 - \alpha$ for a well-calibrated prediction.

116 For a fair comparison, all methods use the same architecture, namely an FNO with 20 hidden channels,
 117 10 modes in the time dimension, and 12 modes in the spatial dimension (2d or 3d respectively), and
 118 generate a predictive distribution of size $M = 100$. Furthermore, we tune the dropout for all methods
 119 separately via grid search, as they highly depend on this parameter. The results for both experiments
 120 can be found in Table 1, while Figure 1 shows an additional analysis of the temporal behavior of the
 121 estimations for the Kuramoto-Sivashinsky equation.

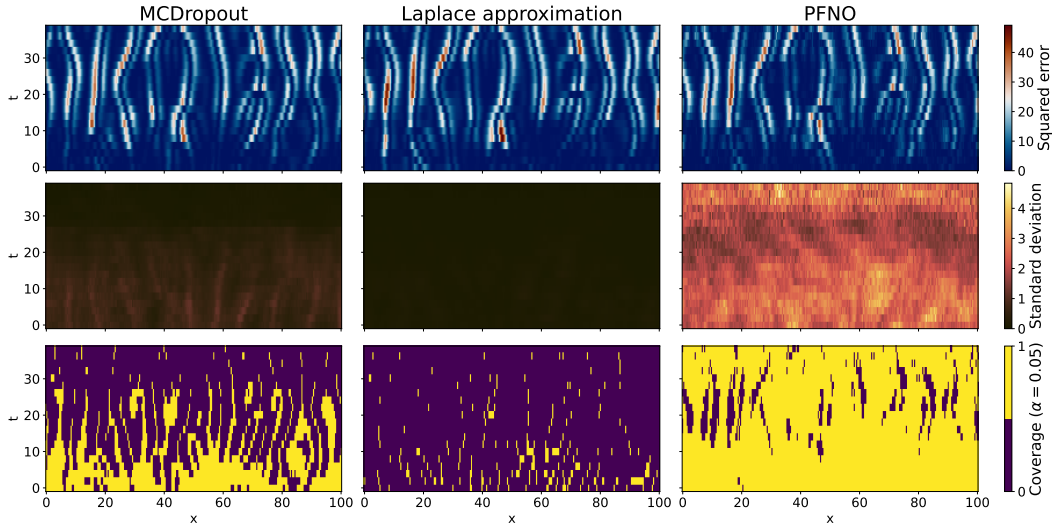


Figure 1: The figure shows the squared error, standard deviation, and 95%-coverage for the different methods on a random test sample of the Kuramoto-Sivashinsky equation. The mean coverage values from left to right are 30.90%, 4.82% and 89.32%.

122 5 Conclusion

123 The PFNO obtains the best fit between the observation and the predictive distribution in terms of the
 124 energy score. Furthermore, for the temperature prediction task, the RMSE is comparable to or even
 125 lower than the other methods, although it is not explicitly minimized by the network. Finally, the
 126 PFNO provides the best-calibrated prediction intervals, although the coverage is generally below the
 127 optimal value. For the temperature prediction task, the performance is significantly worse on the
 128 test set for all models and future research might revolve around making the approaches more robust
 129 against out-of-distribution data. While the Laplace approximation is very easy to use and admits
 130 an approximate analytically available Gaussian distribution, this might not be flexible enough for
 131 complex dynamical systems, if, for example, the uncertainty does not follow a symmetric distribution.
 132 Although it leads to a better mean estimation, as it is based on the MAP estimate, the predictive
 133 uncertainty is not as adequate. The MCDropout method lacks calibration in terms of coverage but
 134 also generally provides a good mean prediction.

135 While our approach shows improved performance, is easy to implement, and can be used with
 136 basically any architecture, it requires an additional training step and more computational power, as
 137 multiple samples are necessary to calculate the loss function. Still, these findings are very promising
 138 and encourage further analysis of neural operators trained with scoring rule minimization for complex
 139 dynamical systems. Some aspects to investigate are different suitable scoring rules, different ways of
 140 generating the samples, as well as ways to improve coverage and calibration of the prediction.

141 **References**

142 C. Bülte, N. Horat, J. Quinting, and S. Lerch. Uncertainty quantification for data-driven weather
143 models. Number arXiv:2403.13458. arXiv, Mar. 2024. doi:10.48550/arXiv.2403.13458.

144 J. Chen, T. Janke, F. Steinke, and S. Lerch. Generative machine learning methods for multivariate
145 ensemble postprocessing. *The Annals of Applied Statistics*, 18(1):159–183, Mar. 2024. ISSN
146 1932-6157, 1941-7330. doi:10.1214/23-AOAS1784.

147 Y. Gal and Z. Ghahramani. Dropout as a bayesian approximation: Representing model uncertainty in
148 deep learning. In M. F. Balcan and K. Q. Weinberger, editors, *Proceedings of the 33rd International
149 Conference on Machine Learning*, volume 48 of *Proceedings of Machine Learning Research*, pages
150 1050–1059, New York, New York, USA, 2016. PMLR.

151 T. Gneiting and A. E. Raftery. Strictly proper scoring rules, prediction, and estimation. *Jour-
152 nal of the American Statistical Association*, 102(477):359–378, 2007. ISSN 0162-1459.
153 doi:10.1198/016214506000001437.

154 N. Kovachki, Z. Li, B. Liu, K. Azizzadenesheli, K. Bhattacharya, A. Stuart, and A. Anandkumar.
155 Neural operator: Learning maps between function spaces with applications to pdes. *Journal of
156 Machine Learning Research*, 24(89):1–97, 2023.

157 Z. Li, N. Kovachki, K. Azizzadenesheli, B. Liu, K. Bhattacharya, A. Stuart, and A. Anandkumar.
158 Fourier Neural Operator for Parametric Partial Differential Equations. Number arXiv:2010.08895.
159 arXiv, May 2021.

160 R. Lyons. Distance covariance in metric spaces. *The Annals of Probability*, 41(5):3284–3305, Sept.
161 2013. ISSN 0091-1798, 2168-894X. doi:10.1214/12-AOP803.

162 E. Magnani, M. Pförtner, T. Weber, and P. Hennig. Linearization Turns Neural Operators into
163 Function-Valued Gaussian Processes. Number arXiv:2406.05072. arXiv, June 2024.

164 L. Pacchiardi, R. A. Adewoyin, P. Dueben, and R. Dutta. Probabilistic forecasting with generative
165 networks via scoring rule minimization. *Journal of Machine Learning Research*, 25(45):1–64,
166 2024.

167 J. Pathak, S. Subramanian, P. Harrington, S. Raja, A. Chattopadhyay, M. Mardani, T. Kurth, D. Hall,
168 Z. Li, K. Azizzadenesheli, P. Hassanzadeh, K. Kashinath, and A. Anandkumar. FourCastNet:
169 A Global Data-driven High-resolution Weather Model using Adaptive Fourier Neural Operators.
170 Number arXiv:2202.11214. arXiv, Feb. 2022. doi:10.48550/arXiv.2202.11214.

171 S. Rasp, S. Hoyer, A. Merose, I. Langmore, P. Battaglia, T. Russel, A. Sanchez-Gonzalez,
172 V. Yang, R. Carver, S. Agrawal, M. Chantry, Z. B. Bouallegue, P. Dueben, C. Bromberg,
173 J. Sisk, L. Barrington, A. Bell, and F. Sha. WeatherBench 2: A benchmark for the next gen-
174 eration of data-driven global weather models. Number arXiv:2308.15560. arXiv, Jan. 2024.
175 doi:10.48550/arXiv.2308.15560.

176 P. I. Renn, C. Wang, S. Lale, Z. Li, A. Anandkumar, and M. Gharib. Forecasting subcritical cylinder
177 wakes with Fourier Neural Operators. Number arXiv:2301.08290. arXiv, Jan. 2023.

178 D. Sejdinovic, B. Sriperumbudur, A. Gretton, and K. Fukumizu. Equivalence of distance-based and
179 RKHS-based statistics in hypothesis testing. *The Annals of Statistics*, 41(5):2263–2291, Oct. 2013.
180 ISSN 0090-5364, 2168-8966. doi:10.1214/13-AOS1140.

181 I. Steinwart and J. F. Ziegel. Strictly proper kernel scores and characteristic kernels on compact
182 spaces. *Applied and Computational Harmonic Analysis*, 51:510–542, Mar. 2021. ISSN 1063-5203.
183 doi:10.1016/j.acha.2019.11.005.

184 T. Weber, E. Magnani, M. Pförtner, and P. Hennig. Uncertainty quantification for fourier neural
185 operators. In *ICLR 2024 Workshop on AI4DifferentialEquations in Science*, 2024.

186 J. Ziegel, D. Ginsbourger, and L. Dümbgen. Characteristic kernels on Hilbert spaces, Banach
187 spaces, and on sets of measures. *Bernoulli*, 30(2):1441–1457, May 2024. ISSN 1350-7265.
188 doi:10.3150/23-BEJ1639.

189 **A Proper scoring rules in separable Hilbert spaces**

190 This section aims to provide more detailed insights into proper scoring rules and generalizations over
 191 separable Hilbert spaces. The results and notations draw mainly on Ziegel et al. [2024], Steinwart and
 192 Ziegel [2021]. Let $(\mathcal{X}, \mathcal{A})$ be a measurable space and let $\mathcal{M}_1(\mathcal{X})$ denote the class of all probability
 193 measures on \mathcal{X} . Let $k : \mathcal{X} \times \mathcal{X} \rightarrow \mathbb{R}$ be a symmetric and positive function referred to as *kernel*
 194 and define $\mathcal{M}_1^k(\mathcal{X}) := \left\{ P \in \mathcal{M}_1(\mathcal{X}) \mid \int_{\mathcal{X}} \sqrt{k(x, x)} dP(x) < \infty \right\}$. A measurable and bounded
 195 kernel is called *characteristic* if the kernel embedding defined by $\Phi(P) := \int k(\cdot, \omega) dP(\omega)$, with
 196 $P \in \mathcal{M}_1^k(\mathcal{H})$ is injective [Steinwart and Ziegel, 2021].

197 For $\mathcal{P} \subseteq \mathcal{M}_1(\mathcal{X})$, a *scoring rule* is a function $S : \mathcal{P} \times \mathcal{X} \rightarrow [-\infty, \infty]$ such that the integral
 198 $\int S(P, x) dQ(x)$ exists for all $P, Q \in \mathcal{P}$. Define the so-called *expected score* as $S(Q, P) :=$
 199 $\int S(Q, x) dP(x) = \mathbb{E}_{X \sim P}[S(Q, X)]$. Then S is called *proper* with respect to \mathcal{P} if

$$S(P, P) \leq S(Q, P), \quad \text{for all } P, Q \in \mathcal{P}, \quad (10)$$

200 and it is called *strictly proper* if equality in (10) implies $P = Q$. For a more detailed overview
 201 compare Gneiting and Raftery [2007]. Proper scoring rules are closely connected to characteristic
 202 kernels, in fact Steinwart and Ziegel [2021] showed that the *kernel score* is strictly proper if and only
 203 if the underlying kernel is characteristic. The kernel score S_k associated with a measurable kernel k
 204 on \mathcal{X} is the scoring rule $S_k : \mathcal{M}_1^k \times \mathcal{X} \rightarrow \mathbb{R}$ defined by

$$S_k(P, x) = \frac{1}{2} \mathbb{E}_P[k(X, X')] - \mathbb{E}_P[k(X, x)] + \frac{1}{2} k(x, x),$$

205 where $x \in \mathcal{X}$ and $X, X' \stackrel{i.i.d.}{\sim} P \in \mathcal{M}_1^k$.

206 We will use the notion of the kernel score to derive a functional version of the commonly used energy
 207 score [Gneiting and Raftery, 2007] and show that it is a strictly proper scoring rule in separable
 208 Hilbert spaces.

209 **Theorem A.1** (Energy score). *Let \mathcal{H} denote a separable Hilbert space. The energy score ES :*
 210 $\mathcal{M}_1^k(\mathcal{H}) \times \mathcal{H} \rightarrow \mathbb{R}$ *defined as*

$$\text{ES}(P, x) := \mathbb{E}_P[\|X - x\|_{\mathcal{H}}] - \frac{1}{2} \mathbb{E}_P[\|X - X'\|_{\mathcal{H}}],$$

211 *with $x \in \mathcal{H}$ and $X, X' \stackrel{i.i.d.}{\sim} P \in \mathcal{M}_1^k$ is strictly proper relative to the class $\mathcal{M}_1^k(\mathcal{H})$.*

212 *Proof.* Lyons [2013, Theorem 3.25] states that every separable Hilbert space is of so-called strong
 213 negative type, which implies the existence of a positive definite *distance kernel* induced by the metric
 214 $\|\cdot\|_{\mathcal{H}}$ given as $k(z, z') = \|z - z_0\|_{\mathcal{H}} + \|z' - z_0\|_{\mathcal{H}} - \|z - z'\|_{\mathcal{H}}$ for some fixed $z_0 \in \mathcal{H}$. Furthermore,
 215 Sejdinovic et al. [2013, Proposition 29] state that the corresponding kernel k is characteristic. Defining
 216 $k_d(z, z') := d(z, z_0) + d(z', z_0) - d(z, z')$, with $d(x, x') := \|x - x'\|_{\mathcal{H}}$ and $z_0 \in \mathcal{H}$ leads to

$$\begin{aligned} S_{k_d}(P, x) &= -\mathbb{E}_P[k_d(X, x)] + \frac{1}{2} \mathbb{E}_P[k_d(X, X')] + \frac{1}{2} k_d(x, x) \\ &= -\mathbb{E}_P[d(X, z_0) + d(x, z_0) - d(X, x)] + \frac{1}{2} \mathbb{E}_P[d(X, z_0) + d(X', z_0) - d(X, X')] \\ &\quad + \frac{1}{2} (d(x, z_0) + d(x, z_0) - d(x, x)) \\ &= \mathbb{E}_P[d(X, x)] - \frac{1}{2} \mathbb{E}_P[d(X, X')] - \frac{1}{2} \mathbb{E}_P[d(X, z_0)] + \frac{1}{2} \mathbb{E}_P[d(X', z_0)] - \mathbb{E}_P[d(x, z_0)] + d(x, z_0) \\ &= \mathbb{E}_P[d(X, x)] - \frac{1}{2} \mathbb{E}_P[d(X, X')] = \text{ES}(P, x) \end{aligned}$$

217 Since k_d is characteristic, by Steinwart and Ziegel [2021] the energy score is strictly proper relative
 218 to the class $\mathcal{M}_1^{k_d}(\mathcal{H})$. □